Mathematical modelling of heat transfer in six-in-line electric furnaces for sulphide smelting

by Y. Pan*, S. Sun*, and S. Jahanshahi*

Synopsis

An efficient and portable mathematical model has been developed for simulating heat transfer in six-in-line slag-resistance-heating electric furnaces for smelting sulphide ores to produce base metals and platinum group metals. This model is a steady-state one relating furnace conditions and performances to various control and input parameters. Some transient effects occurring in electric furnaces are neglected for computation efficiency. This article describes the model development and modelling results. The present model is capable of predicting: (i) temperatures at various locations in a six-in-line furnace, such as slag bath, matte bath, solid charge, freeboard space, freeze lining, cooling water, and air gaps between solid material components, etc. (ii) freeze lining thickness, (iii) smelting rate, and (iv) heat loss rate, etc. A typical feature of the model is that it is easily portable to different application platforms and sufficiently efficient with execution times less than a few seconds. Therefore, it is possible to apply the model for online prediction and control of heat transfer and freeze lining thickness in industrial electric furnaces.

Keywords
electric furnace, six-in-line furnace, smelting, heat transfer, freeze lining.

Introduction

Slag-resistance-heating electric furnaces, either rectangular in shape with six electrodes in line (six-in-line furnace for short) or circular in shape with three electrodes in delta (three-electrode furnace for short), are commonly used for producing base metals and platinum group metals (PGMs). (For simplicity in terminology, we call all of them electric furnaces). However, due to ever-deteriorating quality of feed materials, especially ore concentrates, together with process intensification through increasing electric power input, the furnaces have to withstand more and more challenging operating conditions, leading to elevated furnace temperatures and unstable furnace operations and integrity. In South Africa, for instance, electric furnaces are widely used for smelting sulphide ores to extract base metals and, in particular, the

PGMs. As the output of low Cr_2O_3 (< 1 wt.%) concentrate from the Merensky ore body becomes increasingly tight, the South African PGM producers tend to rely, at least partly, on the UG2 ore, which contains higher levels of Cr_2O_3 (about 5 wt%)[1]. The high Cr_2O_3 content in the feed causes serious operational problems in the electric furnaces[1,2]. Cr_2O_3 in slag can form spinels with high melting points, leading to more viscous slag that is difficult to control. According to Urquhart et al.[3], Cr_2O_3 can precipitate as spinel particles in low-temperature regions close to both ends of electric furnaces (no. 1 and no. 6 electrode cells), as shown in Figure 1. If the slags are highly viscous, more PGMs, along with matte droplets (prills), may be trapped in the slags. These issues force the operator to run the furnaces at higher temperatures, which not only adds to the cost for consumption of electricity and refractories, but also results in unstable furnace integrity by destablizing the freeze lining. Moreover, as shown in Figure 1, the spinel phases rich in Cr_2O_3 tend to lie between the matte and slag layers, which causes electric conduction problems[1,3], lowering the heating efficiency of the electric furnace.

Process intensification by increasing the power input is often used to maintain high productivity. However, this can lead to operational problems, such as low lining life and cooling unit life due to unstable freeze linings, etc. To keep electric furnaces robust under the changing operating conditions and with the degrading quality of raw materials, it

* *CSIRO Process Science and Engineering, CSIRO Minerals Down Under National Research Flagship, Clayton South, Australia.*

Mathematical modelling of heat transfer in six-in-line electric furnaces for sulphide smelting
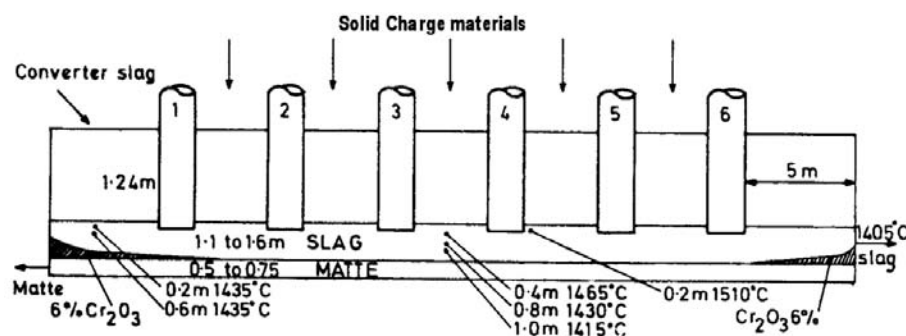

Figure 1—Schematic illustration of 'chromite–problem' in six-in-line furnaces in South Africa (after Urquhart, Rennie, and Rabey[3]

is necessary to find out effective and efficient ways to solve these problems. One possible low-cost solution is the development of simulation tools such as mathematical models that can be conveniently used to efficiently control and optimize the heating process of the electric furnaces so as to maintain smooth, efficient and low-cost furnace operations.

A survey of the literature revealed that mathematical modelling research on heat transfer and fluid flow (with or without coupling of electric fields) in electric furnaces is not extensive, and there are only a few mathematical models available, most of which are based on computational fluid dynamics (CFD) or magnetohydrodynamics (MHD) modelling techniques[4–8]. While these sophisticated models can offer detailed predictions of the fluid flow, heat transfer, and electric fields in the furnaces, they require high computational power to run. Consequently, these models have been used to simulate only portions of an electric furnace, not an entire furnace. Furthermore, they are generally slow to converge and, thus, are inadequate for potential online implementation. Most of the CFD and MHD models require commercial software for implementation, which limits their portability on different application platforms (e.g. furnace control rooms). On the other hand, online predictive models for whole electric furnaces are desperately needed for the industries to stabilize their furnace operations and increase campaign lives. Therefore, alternative models that can simulate the entire furnace and are efficient and portable with a potential for online implementation are necessary, and should be developed to aid the operators obtain timely prediction of performance and better control of their electric furnaces.

The aim of the present work is to develop such models based on alternative mathematical approaches. We expect the models should simulate heat transfer in the whole furnace and should possess the following capabilities:

➤ Prediction of temperatures at various locations in an electric furnace (such as slag bath, matte bath, freeze lining, solid charge, cooling water, freeboard space, air gaps, and various material interfaces, etc.)
➤ Prediction of the thickness of freezing lining
➤ Prediction of the furnace smelting rate and heat loss rate
➤ Aid process problem analysis, control, and optimization

➤ Sufficient accuracy and speed for online implementation
➤ Easy portability to different application platforms and, thus, flexibility in implementation on different electric furnaces.

The current version of the model is a steady-state one. It allows the evaluation of the impact of changing operating parameters on the steady-state conditions of the furnace. The transient behaviour is not yet fully accounted for.

Heat transfer model development

Model principle

In the present work, the heat transfer model was established based on the principle of heat balances in the furnace media (slag, matte, solid charge, and off-gas) and the concept of thermal resistances-in-series for heat transfer in the furnace wall, bottom, and roof, which are comprised of multilayer composite materials. Applications of this principle to the development of heat transfer models for both six-in-line and three-electrode furnaces have been reported elsewhere[9]. The present article describes, in detail, the model development for simulating heat transfer in six-in-line furnaces.

Assumptions

In the present heat transfer model, the following modes of heat transfer and heat exchange are considered to take place in electric furnaces:

➤ Conduction in all solid materials (including porous materials such as the solid charge)
➤ Convection at solid/liquid and liquid/liquid interfaces
➤ Convection and radiation at solid/gas interface
➤ Convection by bulk flows of slag, matte, and off-gas
➤ Heat exchange between the slag bath and newly formed slag and matte droplets by smelting
➤ Heat exchange between the matte bath and the matte droplets passing through the slag bath to enter the matte bath
➤ Heat exchange between the solid charge and reaction gases generated by smelting
➤ Heat exchange between the cold ingress air and hot reaction gases in the freeboard space.

Mathematical modelling of heat transfer in six-in-line electric furnaces for sulphide smelting

In order to mathematically model the abovementioned heat transfer phenomena in electric furnaces, some general assumptions are made:

➤ Steady-state heat transfer
➤ Perfect contact between neighbouring solid material components, except between freeze lining and cooling units, where the formation of air gaps is considered
➤ Thermal equilibrium between the slag bath and the newly formed slag and matte droplets descending from the solid charge layer
➤ Thermal equilibrium between the matte bath and the matte droplets descending from the slag bath
➤ Thermal equilibrium between the solid charge and the reaction gases passing through the solid charge layer to enter the freeboard space
➤ Perfect mixing between ingress air and reaction gases (evolving from the solid charge layer) in the freeboard space
➤ Electrodes neglected, and uniform dissipation of the heat generated by electricity into the whole volume of the slag bath
➤ No heat exchange considered between the electrodes and the furnace media (e.g. slag bath, solid charge, and off-gas, etc.)
➤ Thermal effects of chemical reactions were considered as an independently adjustable input parameter.

The assumption of uniform dissipation of the heat into the whole volume of the slag bath obviously misses the fact that the slag close to the electrodes is hotter than the rest of the slag bath due to non-uniform current distribution, for instance. Further model refinement in this area will be considered in future work.

Furnace geometry and material configuration

Figure 2 schematically illustrates the model representation of a six-in-line furnace. As indicated, the furnace is geometrically considered as an assembly of a number of cells, separated by hypothetical planes shown by the dashed lines in Figure 2. Each cell has one electrode and is termed an electrode cell. Thus, a six-in-line furnace is comprised of six electrode cells. The slag tapholes are assumed to be located in the end wall of no. 6 electrode cell, whereas the matte tap holes are in the end wall of no. 1 electrode cell. The off-gas uptakes are assumed to be located at both ends of the electric furnace. For simplicity, the tapholes and material charging holes (in the furnace roof), as well as off-gas uptakes, are not shown in Figure 2. In addition, the outer surface of the furnace bottom steel shell plate is assumed to be cooled by forced air convection at a uniform velocity of, for example, 10 m/s. By taking advantage of mirror symmetry in geometry about the central vertical plane along the longitudinal direction of the furnace (A–A plane in Figure 2(b)), only half of the furnace is considered in the heat transfer model.

Figure 2 also depicts the furnace material configuration. According to this figure, each electrode cell consists of the following material components:

➤ In vertical direction from the slag bath downwards to the atmosphere: liquid slag bath, matte bath, bottom refractory, bottom insulation layer, and bottom steel shell plate
➤ In vertical direction from the slag bath upwards to the atmosphere: liquid slag bath, solid charge layer, freeboard space (off-gas), and roof refractory
➤ In horizontal direction from the slag bath to the atmosphere: liquid slag bath, solid slag layer (freeze lining), inner copper shell (or block) of cooling unit, cooling water, and outer copper shell of cooling unit
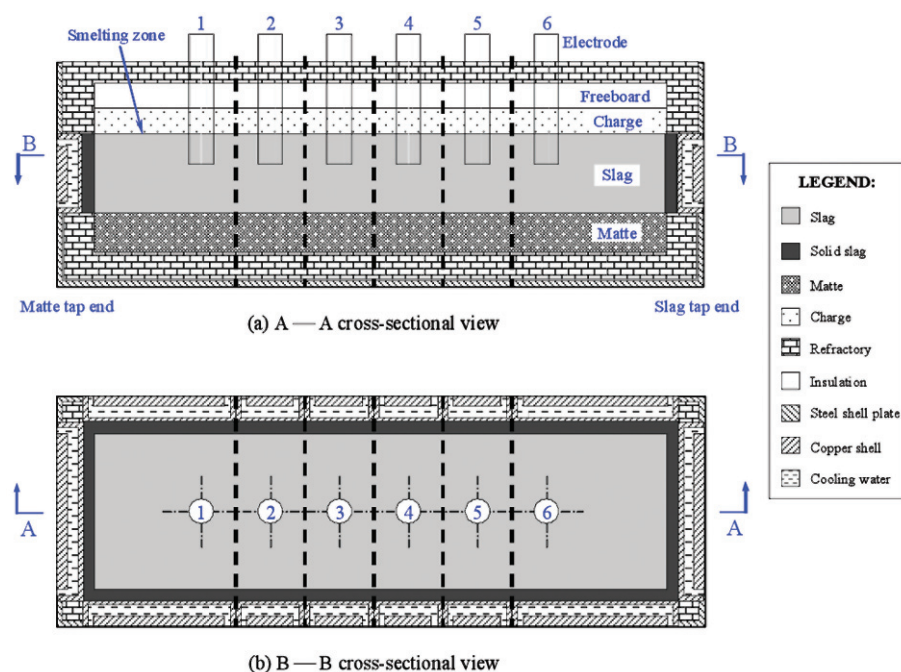

Figure 2—Model representation of a six-in-line furnace

Mathematical modelling of heat transfer in six-in-line electric furnaces for sulphide smelting

➤ In horizontal direction from the matte bath to the atmosphere: matte bath, sidewall refractory, sidewall insulation layer, and sidewall steel shell plate
➤ In horizontal direction from solid charge layer to the atmosphere: solid charge, sidewall refractory, and sidewall steel shell plate
➤ In horizontal direction from freeboard space to the atmosphere: freeboard space, sidewall refractory, and sidewall steel shell plate.

Table I gives, as an example, material dimensions and configurations of a six-in-line furnace simulated by the present heat transfer model, and Table II lists the thermophysical properties of the materials used by the heat transfer model.

Smelting zone

In electric furnaces, the smelting zone is the region where solid charge materials are smelted, at a fixed temperature depending on the chemistry of the charge materials, into liquid slag droplets, liquid matte droplets, and reaction gases. It is generally a thin layer between liquid slag bath and solid charge layer. The characteristics of this zone were described by Sheng *et al.* for nickel smelting [6]. In the present modelling work, we define the interface between slag bath and solid charge as the smelting zone, as indicated in Figure 2(a).

Bulk material flows

Figure 3 schematically depicts the defined flow directions of the bulk fluids, such as liquid slag, liquid matte, gaseous products due to smelting (reaction gases), and ingress air as well as off-gas. As indicated, the slag droplets produced in the smelting zone immediately join in the slag bath and exchange heat with it; the matte droplets produced in the smelting zone first pass through and exchange heat with the slag bath, and then enter the matte bath and exchange heat with the matte bath; and the reaction gases generated in the smelting zone flow upward through the porous solid charge layer, exchange heat with it and then enter the freeboard space where they meet with the ingress air to form the off-gas.

Furthermore, as seen from Figure 3, the bulk slag flows in the longitudinal direction toward the slag tap end of the furnace while, as an assumption, the bulk matte flows in the opposite direction toward the matte tap end of the furnace at a rate corresponding to the average production rate. (It should be borne in mind that, in practice, for six-in-line furnaces the slag is normally tapped continuously but the matte normally tapped periodically in batches, resulting in some transient effects due to the gradual increase of matte bath volume.) The hot reaction gases evolving from the solid charge mix with the cold air infiltrating through the furnace roof (via charging holes and electrode holes, etc.) to form the off-gas, which flows in opposite directions toward the uptakes, which are assumed to be located in both ends of the furnace.

Table I

Dimensions and material layer thicknesses of a six-in-line furnace considered in the heat transfer model

Items	Dimension (m)
Furnace total (outer) length	31.91
Furnace total (outer) width	10.42
Furnace total (outer) height	3.0
Thickness of refractory layer	0.5
Thickness of insulation layer	0.01
Thickness of steel shell plate	0.04
Thickness of copper shell of cooling unit	0.04
Height of slag bath	0.9
Height of matte bath	0.4
Height of charge layer	0.3
Height of freeboard space	0.3
Distance between axis of neighbouring electrodes	3.81
Distance between no. 6 electrode axis and wall of slag tapping end	6.4
Distance between no. 1 electrode axis and wall of matte tapping end	5.2

Table II

Thermophysical properties of materials used in the heat transfer model

Material Unit	Density kg/m³	Heat capacity J/kg·K	Thermal conductivity W/m·K	Viscosity kg/m·s	Thermal expansion coefficient 1/K	Reference
Liquid slag	3200	1250	8	0.3	2.7×10^{-4}	[6]
Matte	4500	720	17	0.05	1.0×10^{-4}	[6]
Solid slag	3500		5			Estimation
Solid charge	2500		0.5			Estimation
Refractory	3000		2			Estimation
Insulation layer	3000		0.1			Estimation
Steel shell plate	7850		60			[12]
Cooling unit copper	8900		400			[12]
Cooling water	990.22	4183	0.637	9.0×10^{-4}	1.4×10^{-4}	[12]
Air at 25°C*	1.188	1005	0.026	1.8×10^{-5}	3.7×10^{-3}	[12]

*Assuming reaction gas and off-gas have the same thermophysical properties as air

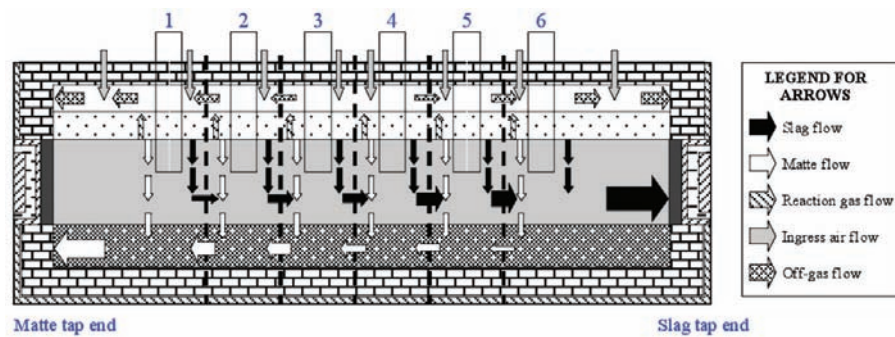# Mathematical modelling of heat transfer in six-in-line electric furnaces for sulphide smelting

Figure 3—Schematic illustration of bulk material flows in six-in-line furnaces assumed in the heat transfer model (see Figure 2 for material legend)

Mathematical formulation

General heat balance equation

In the present modelling work, at steady state, a general heat balance equation for a bulk material (slag bath, matte bath, solid charge layer or off-gas above the solid charge layer) in an electrode cell of a six-in-line furnace can be written as

$$\text{Net heat input rate} = \sum_j \frac{T_{bulk} - T_b}{\sum_i R_i} \qquad [1]$$

where, T_{bulk} is the average temperature of a bulk material in question (such as slag, matte, solid charge or off-gas); T_b is the boundary temperature; j denotes the direction of heat transfer; i stands for a material layer involved in the electrode cell; and R_i is the thermal resistance of the ith material layer or the interface between this material layer and the fluid flowing over it.

The right-hand side of Equation [1] is a general representation of the rate of heat lost, in different directions indicated by j, to the atmosphere or to the cooling water, in which T_b is defined as below:

(1) For heat losses from the slag bath to the cooling units, T_b is the inflow cooling water temperature
(2) For heat losses from a bulk material to the atmosphere, T_b is the atmosphere (room) temperature.

Equation [1] states that at steady state a net heat input into a bulk material in an electrode cell dissipates through the bounding materials to the atmosphere and cooling water. Based on Equation [1], heat balance equations for the individual bulk materials can be easily derived. Examples are given in the following sections.

Heat balance in the slag bath

As shown in Figure 2, the slag bath is bounded by the matte bath below, the freeze lining in the sidewall, and the solid charge layer above. As mentioned earlier, the slag/charge interface is defined as the smelting zone where the solid charge is smelted into slag droplets, matte droplets, and reaction gases. Therefore, at steady state, a heat balance equation for the slag bath can be written as follows:

$$Q_{sm} + Q_{m-conv} + Q_{m-droplets} = \sum_j \frac{T_m - T_a}{\sum_i R_i} \qquad [2]$$

where, Q_{input} is the effective electric energy input rate (power) into slag bath in an electrode cell (W); Q_{s-conv} is the net convection heat flow rate transported by the bulk slag flow from the neighbouring electrode cells; $Q_{droplets}$ is the net sensible heat flow rate brought by the descending slag and matte droplets produced at the slag/charge interface (smelting zone); Q_{sc} is the convection heat flow rate from the slag bath to the slag/charge interface; Q_{sm} is the convection heat flow rate from the slag bath to the matte bath; T_s is the average temperature of the bulk slag in an electrode cell; and $T_{w,in}$ is the temperature of the inflow water into cooling units.

The term on the right-hand side of Equation [2] stands for the heat flow rates through the sidewalls (in electrode cells nos. 2 to 5) or the side and the endwalls (in electrode cells nos. 1 and 6) from the slag bath, through the multilayer materials (i.e. freeze lining, copper shell of cooling unit, and, if any, air gap in between), to the cooling water. The heat loss through the outer copper shell of the cooling unit is ignored.

Heat balance in the matte bath

The matte bath is bounded by the refractory in the bottom and in the sidewall and by the slag bath on the top. At steady state, a heat balance equation for the matte bath can be written as

$$Q_{sm} + Q_{m-conv} + Qm - droplets = \sum_j \frac{T_m - T_a}{\sum_i R_i} \qquad [3]$$

where, Q_{m-conv} is the net convection heat flow rate transported by the bulk matte flow from the neighbouring electrode cells; $Q_{m-droplets}$ is the sensible heat flow rate brought by the matte droplets descending from the slag bath; T_m is the average temperature of the bulk matte in an electrode cell; and T_a is the ambient (atmosphere or room) temperature.

The term on the right-hand side of Equation [3] stands for the heat flow rates through the side and the bottom walls

Mathematical modelling of heat transfer in six-in-line electric furnaces for sulphide smelting

(in electrode cells nos. 2 to 5) or the side, the bottom, and the end walls (in electrode cells nos. 1 and 6) from the matte bath, through the multilayer materials (i.e. refractory, insulation layer, and steel shell plate) to the atmosphere.

Heat balance in the solid charge

The solid charge is bounded by the slag bath below, the refractory in the sidewall, and the freeboard space above. A heat balance equation for the solid charge layer can be written as

$$Q_{scc} + Q_{c-cond} + Q_{gas} - Q_{cf} = \sum_j \frac{T_c - T_a}{\sum_i R_i} \qquad [4]$$

where, Q_{scc} is the conduction heat flow rate from slag/charge interface to the centre of the solid charge layer; Q_{c-cond} is the net conduction heat flow rate in the solid charge from the neighbouring electrode cells; Q_{gas} is the net heat flow rate absorbed by the solid charge from the reaction gases generated by smelting at the slag/charge interface; Q_{cf} is the convection and radiation heat flow rate from the top surface of the solid charge layer to the freeboard space; and T_c is the temperature at the centre of the solid charge layer in an electrode cell.

The term on the right-hand side of Equation [4] stands for the heat flow rates, in two directions (along the length and the width of the furnace), from the solid charge through the multilayer composite materials (i.e. refractory and steel shell plate) to the atmosphere.

Heat balance in the freeboard space

The freeboard space is enclosed by the solid charge below, the refractory in the sidewall, and the refractory in the roof. It is a volume filled with the off-gas formed by a mixture of the reaction gases (generated by smelting) and the ingress air (infiltrated from the atmosphere). A heat balance equation for the freeboard space reads:

$$Q_{cf} + Q_{g-conv} + Q'_{gas} - Q_{ingress-air} = \sum_j \frac{T_f - T_a}{\sum_i R_i} \qquad [5]$$

where, Q_{g-conv} is the net convection heat flow rate transported by bulk off-gas flow in the freeboard space from the neighbouring electrode cells; Q'_{gas} is the net heat flow rate transported by the reaction gases evolving through the solid charge layer into the freeboard space; $Q_{ingress-air}$ is rate of heat absorbed by ingress air in the freeboard space; and T_f is the average temperature of the bulk off-gas in an electrode cell.

The term on the right-hand side of Equation [5] stands for the heat flow rates from the freeboard space to the atmosphere through the sidewalls and the roof. In addition, a fixed volumetric flow rate of the ingress air is introduced into each electrode cell.

In the present modelling work, we aim to solve Equation [1] or Equations [2] to [5], constrained by appropriate boundary conditions, to obtain the following results:

➤ Average temperatures of all bulk fluid phases (e.g. liquid slag, liquid matte and off-gas, etc.)
➤ Average temperatures of all solid material components
➤ Temperatures at various interfaces (e.g. fluid/fluid, fluid/solid and solid/solid interfaces)
➤ Freeze lining thickness
➤ Smelting rate
➤ Heat loss rate, etc.

Calculation of the freeze lining thickness

Under the steady-state heat transfer condition, the thickness of the freeze lining layer can be calculated in a straightforward manner as follows

$$L_{freeze} = \frac{k_{ss} A_{sw} (T_{sol} - T_{sw})}{Q_{sw}} \qquad [6]$$

where, Q_{sw} is the convection heat flow rate from the bulk liquid slag to the surface of the freeze lining layer; T_{sol} is the solidus of the freeze lining (i.e. solid slag), which is set to 132 K for nickel smelting[6]; T_{sw} is the temperature of the interface between the freeze lining layer and the copper shell of the cooling unit for perfect contact conditions, or the cold face temperature of the freeze lining layer if there is an air gap between the freeze lining and the copper shell of the cooling unit; k_{ss} is the thermal conductivity of the freeze lining; and A_{sw} is the area of heat transfer between the freeze lining and the cooling unit.

Calculation of the furnace smelting rate

The electric furnace smelting rate is defined as the amount of solid charge that is smelted per unit time. This parameter is obtained based on the net rate of heat flow consumed for smelting and the heat required for smelting per ton of solid charge (defined as charge smelting heat), i.e.

$$G_{smelt} = \frac{Q_{smelt}}{H_{smelt}} \qquad [7]$$

where, G_{smelt} is the charge smelting rate in an electrode cell; H_{smelt} the charge smelting heat (for nickel smelting, H_{smelt} is evaluated to be 1.326 MJ/t, using the data reported by Sheng *et al.*[6]); and Q_{smelt} the net rate of heat flow consumed for smelting the solid charge, which is defined as the difference between the rate of heat flow supplied from slag bath to the slag/charge interface (i.e. smelting zone) and the rate of heat flow consumed for heating solid charge, slag and matte, and by conduction to the centre of the solid charge layer, i.e.

$$Q_{smelt} = Q_{sc} - Q_{scc} - Q_c - Q_s - Q_m \qquad [8]$$

The heat flow rate from the slag bath to the smelting zone, Q_{sc}, is calculated as

$$Q_{sc} = \frac{T_s - T_{smelt}}{R_{sc}} \qquad [9]$$

where T_{smelt} is the smelting zone temperature, which is set to 1373 K for nickel smelting[6]; and R_{sc} the heat transfer resistance at the slag/charge interface, which is a function of heat transfer coefficient and area of the slag/charge interface.

The heat flow rate from the slag/charge interface by conduction to the centre of the solid charge layer, Q_{scc}, is calculated as

$$Q_{scc} = \frac{T_{smelt} - T_c}{R_{scc}} \qquad [10]$$

where, R_{scc} is the conduction heat transfer resistance between the slag/charge interface and the centre of the solid charge layer.

Q_c is the rate of heat flow consumed for heating the solid charge to the smelting zone temperature:

$$Q_c = G_{smelt} C_{pc} (T_{smelt} - T_a) \qquad [11]$$

where C_{pc} is the heat capacity of solid charge.

Q_s is the rate of heat flow consumed for heating the newly produced slag droplets from the smelting zone temperature to the slag bath temperature:

$$Q_s = G_s C_{ps} (T_s - T_{smelt}) \qquad [12]$$

where G_s is the slag production rate and C_{ps} the heat capacity of liquid slag.

Q_m is the rate of heat flow consumed for heating the newly produced matte droplets from the smelting zone temperature to the slag bath temperature:

$$Q_m = G_m C_{pm} (T_s - T_{smelt}) \qquad [13]$$

where G_m is the matte production rate and C_{pm} the heat capacity of liquid matte.

In the present modelling work, it is assumed that the smelting of solid charge generates mainly three forms of products, i.e. slag, matte, and gas. Based on unpublished mass balance calculations on smelting copper- and nickel-bearing sulphide ores, the weight fractions in percentages of slag, matte, and gas in the total smelting products are estimated to be 72.7%, 19.1%, and 8.2%, respectively. For PGM smelting, however, different mass balance calculations should be used to obtain such data.

The total furnace smelting rate is the summation of the smelting rates (G_{smelt}) of all the six electrode cells in an electric furnace. Likewise, the total furnace heat loss rate is the summation, also over all the six electrode cells, of the heat loss rates through furnace bottom, wall, and roof to the atmosphere, through the freeze lining layer to the cooling water and through the solid charge layer to the off-gas flowing out of the furnace.

Calculation of the thermal resistances

The thermal resistance, R_i, involved in Equations [1] to [5] can be calculated as
   (i) for a flat layer of solid material,

$$R_i = \frac{L_i}{k_i A_i} \qquad [14]$$

   (ii) at liquid/liquid or liquid/solid interface (such as liquid slag/matte, liquid slag/solid slag, liquid slag/solid charge, matte/refractory, or cooling water/copper shell of cooling unit),

$$R_i = \frac{1}{h_i A_i} \qquad [15]$$

   (iii) at steel shell plate/ambient air interfaces,

$$R_i = \frac{1}{\left[h_i + \varepsilon \sigma \left(T_{surf} + T_a \right) \left(T_{surf}^2 + T_a^2 \right) \right] A_i} \qquad [16]$$

   (iv) at solid/gas interfaces enclosing internal cavities (such as freeboard space and air gaps between layers of solid materials),

$$R_i = \frac{1}{\left[h_i + F_{ij} \varepsilon \sigma \left(T_{surf,i} + T_{surf,j} \right) \left(T_{surf,i}^2 + T_{surf,j}^2 \right) \right] A_i} \qquad [17]$$

In the present heat transfer model, only the air gap formed between the freeze lining and the copper shell of cooling unit is considered, and the heat transfer by convection inside the air gaps is neglected. In addition, the radiation heat transfer through all condensed phases is also neglected.

Calculation of the heat transfer coefficients

As seen from Equations [15] to [17], convection heat transfer coefficients are involved in the calculations of the heat transfer resistances of various liquid/liquid and fluid/solid interfaces. In the present model, we adopted corrected empirical dimensionless correlations to evaluate the heat transfer coefficients for various interfaces involving fluids, i.e.

$$h = f \frac{k}{L} Nu \qquad [18]$$

where, h is heat transfer coefficient; k is thermal conductivity L is a characteristic length of the interface; Nu is the Nusselt number; and f is a correction factor for each interface. (For clarity, in Equation [18] the material identity, i, as a subscript, is omitted.)

The heat transfer coefficient correction factor f should be evaluated using measured data (e.g. temperatures) on the electric furnaces to be modelled. As an example, Table III gives a set of f values obtained, based on published data[6] and by means of trial and error, for various interfaces in a production six-in-line furnace of Xstrata plc operated at Sudbury (formerly Falconbridge Limited), Ontario, Canada. By using this set of f values, a good match was obtained between the model-predicted temperatures vertically across the slag and matte baths and the measurements reported by Sheng and Irons[6], as shown in Figure 4. In addition, based on the same set of f values, a reasonable agreement between the predicted furnace charge smelting rate, as a function of total furnace power input, and that reported by Sheng and Irons[6] was also reached, as shown in Figure 5.

The Nusselt number in Equation [18] is obtained from the following empirical dimensionless correlations based on natural convection flows[10,11]:
   (i) for all vertical interfaces (e.g. interfaces between liquid slag/freeze lining, matte/sidewall refractory and sidewall shell plate/ambient air, etc.):

Table III

Heat transfer coefficient correction factors for an industrial six-in-line furnace

Interface	Correction factor (f)
Slag/freeze lining	0.15
Slag/matte (slag side)	0.15
Slag/matte (matte side)	0.1
Slag/solid charge	0.31
Matte/side refractory	0.1
Matte/bottom refractory	0.1
Solid charge/freeboard off-gas	0.1
Water/copper of cooling unit	1.0
Side shell plate/ambient (matte section)	1.0
Side shell plate/ambient (charge section)	1.0
Bottom shell plate/ambient	1.0
Off-gas/roof refractory	1.0
Off-gas/side refractory	1.0
Roof refractory/ambient	1.0
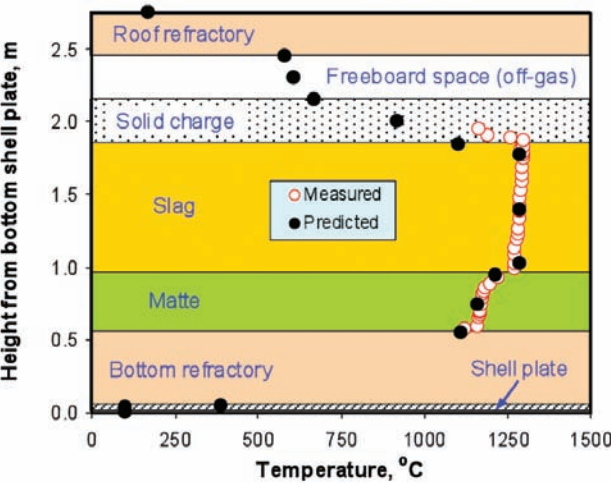
Figure 4—Comparison between model predicted temperatures (solid circles) and measurements (open circles)[6]
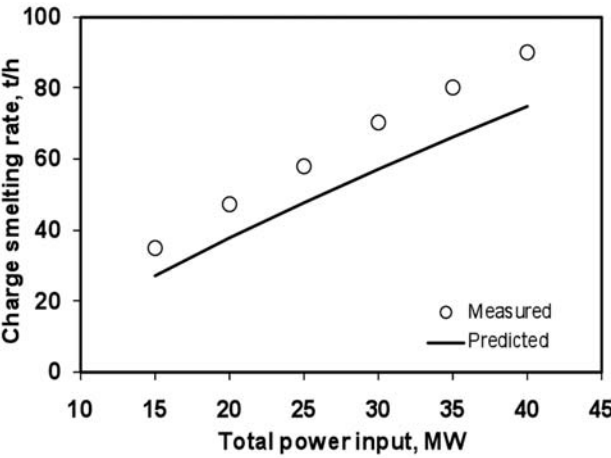
Figure 5—Comparison between model predicted charge smelting rates (line) and measurements (open circles)[6]

$$Nu = \frac{0.902\sqrt{Pr}}{(0.861+Pr)^{1/4}}\left(\frac{Gr}{4}\right)^{1/4} \qquad [19]$$

where Nu, Pr, and Gr are the Nusselt number, the Prandtl number and the Grashof number, respectively

(ii) for horizontal interfaces:

if the interfaces are hot and facing upward or cold facing downward (e.g. interfaces between liquid slag/solid charge, and roof refractory /ambient air, etc.)

$$Nu = 0.14(Gr\cdot Pr)^{1/3} \qquad \left(2\times10^7 \le Gr \le 3\times10^{10}\right) \quad [20]$$

or

$$Nu = 0.54(Gr\cdot Pr)^{1/4} \qquad \left(1\times10^5 \le Gr < 2\times10^7\right) \quad [21]$$

If the interfaces are hot and facing downward or cold facing upward (e.g., interfaces between slag/matte and matte/bottom refractory, etc.):

$$Nu = 0.27(Gr\cdot Pr)^{1/4} \qquad [22]$$

(iii) for interfaces where only forced convection applies, the following dimensionless correlations, derived from reference[13], are employed:

$$Nu = 0.664\,Re^{1/2}\,Pr^{1/3} \qquad \left(Re < 2\times10^5\right) \qquad [23]$$

or

$$Nu = 0.036\,Re^{0.8}\,Pr^{0.43} \qquad \left(Re \ge 2\times10^5\right) \qquad [24]$$

where Re is the Reynolds number.

Heat transfer in the cooling unit

For heat transfer in water cooling units, special treatments were made for evaluating the heat transfer resistance between copper shell and water and the relevant convection heat transfer coefficient. In the present modelling work, the water cooling unit is assumed to be a wall made of a snakelike copper pipe with water running through it, as schematically illustrated in Figure 6. Based on the geometrical and material configurations shown in this figure, the overall thermal resistance for the interface between the copper shell (pipe wall) and water can be derived, by integration over the total length of the water pipe, as
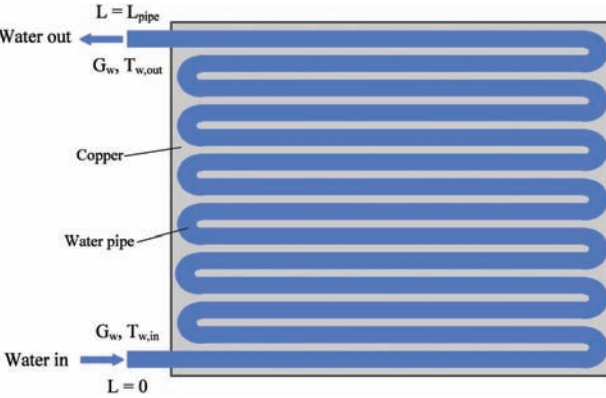

Figure 6—Schematic illustration of water cooling unit considered in the heat transfer model

$$R_{cw} = \cfrac{1}{G_w C_w \left(1 - e^{-\frac{\pi D_w h_w}{G_w C_w} L_{pipe}}\right)} \qquad [25]$$

The convection heat transfer coefficient between water and pipe wall is calculated as

$$h_w = f_w \frac{k_w}{D_w} Nu_w \qquad [26]$$

where the Nusselt number is obtained from the following empirical dimensionless correlation[10]

$$Nu_w = 0.026\, Re_w^{0.8}\, Pr_w^{1/3} \left(\frac{\mu_b}{\mu_0}\right)^{0.14} \qquad [27]$$

Based on these equations, the temperature of water flowing out of the cooling unit can be calculated by using the following equation:

$$T_{w,out} = T_{cw} - \left(T_{cw} - T_{w,in}\right)e^{-\frac{\pi D_w h_w}{G_w C_w} L_{pipe}} \qquad [28]$$

For the meanings of all the symbols involved in Equations [14] through [28], see the Appendix.

Modelling method, efficiency and model portability

In the present work, the heat transfer model was established by numerically solving Equation [1] or Equations [2] to [5]. Gauss-Seidel iteration method was used to obtain primary solutions T_s, T_m, T_c and T_f, together with various interfacial temperatures (e.g., T_{sw} and T_{surf}, etc.), from which other parameters, shuch as freeze lining thickness and charge smelting rate, etc., can be calculated using Equations [6] and [7], respectively. The model was developed into an in-house computer program coded in DIGITAL Visual Fortran 90, which generates executables that can run in all personal computers with Microsoft™ Windows®. The model can be executed both in a GUI and in a command line. In the case of using a GUI, a user-friendly Excel® spreadsheet was designed, using Microsoft™ Visual Basic Scripts®, where all data input and output and execution of the program can be made. It saves input/output data in files of both XLS and TXT formats. Users can type in their input data in worksheets named in different categories like 'Furnace Dimensions' and 'Material Properties', etc. Then, the users can submit their input data (by pressing 'SAVE INPUT DATA' button), execute the model (by pressing 'RUN' button), check the results (by pressing 'OUTPUT RESULT' button), all in one Excel worksheet. Furthermore, some typical graphics/charts can be automatically generated in Excel for user's convenience and at user's choice, such as slag, matte, solid charge, and off-gas temperatures, freeze lining thickness, slag and matte production rates, etc. In addition, an online help function (accessed by pressing the 'HELP' button) was also designed should the users need help to use the model. Therefore, the model is easily portable and can be executed on a wide variety of computing platforms with Microsoft Windows with an Office suite including Excel. Moreover, the model is also sufficiently efficient, with execution times of less than a few seconds even on ordinary personal computers. Therefore, the model can potentially be applied online for prediction and control of the heating on production electric furnaces in industries.

Results and discussion

Predicted temperatures of slag and matte in a six-in-line furnace

Figure 7 shows the predicted average temperatures in the slag and matte baths for each electrode cell of a six-in-line furnace. The furnace has a total power input of 22 MW. This electric power is uniformly distributed to the six electrodes. That is, each electrode cell receives 3.67 MW heating power. Under this condition, it can be seen from Figure 7 that the resultant average temperatures in the bulk slag and matte are non-uniform along the length of the furnace. The temperatures in the end electrode cells (i.e. no.1 and no.6 electrode cells) are noticeably lower than those in the middle electrode cells. The reason is self-evident in that, as depicted by Figure 2, the no. 1 and no. 6 electrode cells have larger volumes (and hence lower average power density) and more heat transfer surfaces (walls) than the middle electrode cells. This feature of the results is commonly found in practice and could be the major reason why chromite spinel precipitation normally appears at the ends of some electric furnaces operated in South Africa, as depicted by Figure 1.

Predicted temperatures of solid charge and off-gas in a six-in-line furnace

Figure 8 shows the predicted solid charge temperature and off-gas temperature in each electrode cell of a six-in-line furnace, corresponding to the slag and matte temperatures shown in Figure 7. It can be seen that, unlike the distributions of slag and matte temperatures, the solid charge temperature is quite evenly distributed along the length of the furnace. This is because, even though the slag temperatures in the end electrode cells are lower than those in the
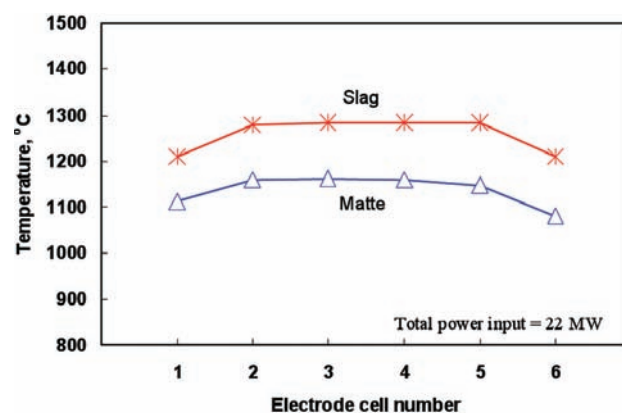

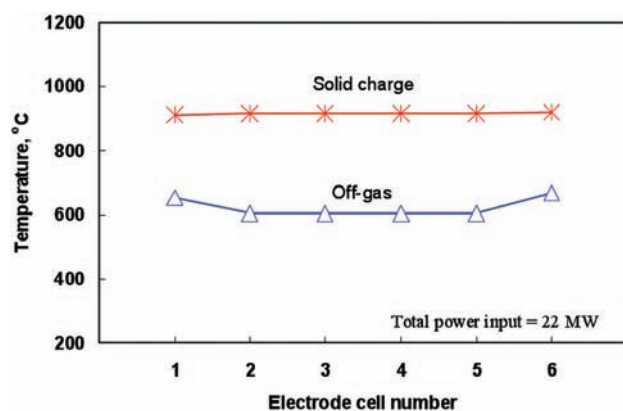Figure 7—Predicted bulk slag and matte temperatures in a six-in-line furnace

Figure 8—Predicted solid charge and off-gas temperatures in a six-in-line furnace

middle cells, the off-gas temperatures in these electrode cells are higher than those in the middle cells and, thus, the combined thermal effects of the slag bath and the off-gas lead to a nearly uniform temperature distribution in the solid charge layer along the length of the furnace. The reason why the off-gas temperatures in no.1 and no.6 electrode cells are higher than those in the middle cells is due to the assumptions that the off-gas uptakes are arranged in these cells and the same amount of leakage air is assumed for each electrode cell.

Predicted freeze lining thickness in a six-in-line furnace

Figure 9 shows the predicted thickness of the freeze lining along the long wall of a six-in-line furnace under the same power input condition shown in Figures 7 and 8. We can see that the freeze lining thickness is closely related to the slag temperature distribution along the length of the furnace (c.f. Figure 7). The freeze lining is much thinner in the middle electrode cells than in the end electrode cells, because the slag temperature is higher in the former cells but lower in the latter cells. For very high power input or extreme bulk slag temperatures, more attention should be paid to the cooling in the middle electrode cells of electric furnaces. In addition, special flow and heat transfer conditions near the tapholes are obviously additional factors of importance.

Predicted smelting rate in a six-in-line furnace

The predicted smelting rate of solid charge as a function of the total power input was shown in Figure 5. For the purpose of model verification, the measured solid charge smelting rates reported by Sheng et al.[6] are also included in the figure for comparison, which indicate that the model underestimates the smelting rate to some extent depending on the power input, showing the discrepancies become larger for a higher power input. The reason for such discrepancies are: (i) a primary cause being that the results given in Figure 5 exclude the effect of coke combustion in the electric furnace investigated by Sheng et al.[6], and (ii) a secondary cause

being that, due to natural convection, a temperature gradient exists across the height of the slag bath, leading to a higher temperature in the vicinity of the smelting zone than the average temperature of the bulk slag. Thus, Equation [9] generally underestimates the heat flow rate (Qsc) to the smelting zone. Both factors are enhanced at a higher power input resulting in a larger discrepancy between the model predictions and the measurements.

Figure 5 also shows that the smelting rate increases nearly linearly with the increase of the power input. A 10 MW increase of power input will lift the smelting rate by about 20 t/h. This implies that the process intensification by increasing power input is an effective way to enhance productivity. However, as indicated by Figure 10, which is plotted based on the same data as shown in Figure 5, in terms of specific power consumption (i.e. total power input rate divided by total charge smelting rate), both predicted and measured smelting rates exhibit a minimum with respect to the power input. This demonstrates that there exists an economic range of power input, in which the lowest specific power consumption could be reached.

The reason for the existence of minimum specific power consumption could be two-fold: (i) in electric smelting processes, a minimum power input is necessary to keep the bulk slag temperature always above the smelting temperature (otherwise, no smelting would occur and thus the smelting rate would be zero), and (ii) the relationship between the smelting rate and the power input is not strictly proportional, but a slightly convex and monotonic-rise curve. The first factor dominates the downward trend at low smelting rates, while the second factor governs the rise in specific power consumption at high smelting rates. The second factor results from the non-linearity in the governing equations of heat transfer, i.e., Equation [1] or Equations [2] to [5], in which some thermal resistances are complex functions of temperature. Typically, as implied by Equations [19] to [22], the heat transfer coefficients computed by the present model are nonlinear functions of temperature. Since these two factors are intrinsic to all electric furnaces, it can thus be
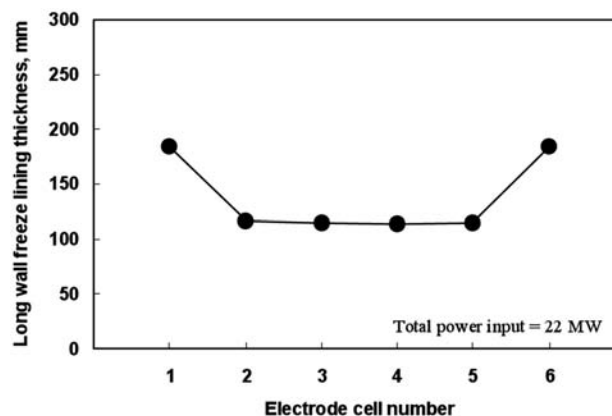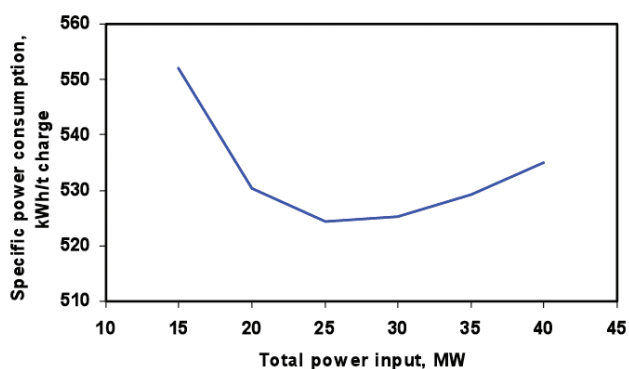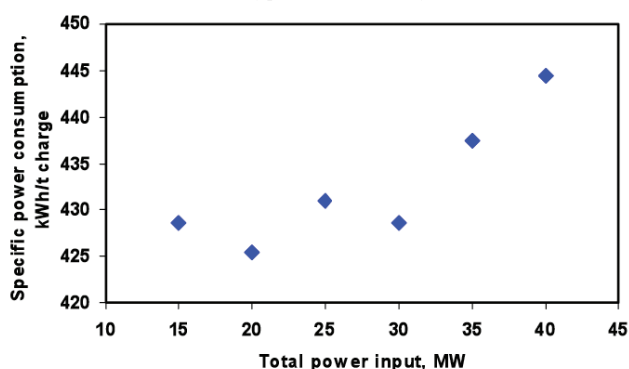

Figure 9—Predicted freeze lining thickness on the long sidewall in a six-in-line furnace

Mathematical modelling of heat transfer in six-in-line electric furnaces for sulphide smelting

(a) Predicted influence of power input on specific power consumption for smelting per ton of solid charge

(b) Measured influence of power input on specific power consumption for smelting per ton of solid charge (derived from data of Sheng and Irons)[6]

Figure 10—Predicted and measured specific power consumption as a function of total power input in a six-in-line furnace

inferred that there is likely to be an economical range of power input, in which minimum specific power consumption could be realized. According to Figure 10, this economical power input range may be found to be 20–30 MW. Of course, applying such an economical power input doesn't guarantee a high productivity. Therefore, a compromise between productivity and specific power consumption, resulting in a net gain in profit, would be highly recommended in practice. The relationship between the power input and the specific power consumption will be further investigated in the future.

Predicted heat loss rate in a six-in-line furnace

Figure 11 illustrates the ratio (in percentage) between the total heat loss rate and the total power input as a function of the total power input for a six-in-line furnace. We can see from this figure that the total heat loss as a percentage of the total power input decreases with increasing of the power input. This suggests that at a high power input level a smaller fraction of the input power is lost to the surroundings. However, as indicated by Figure 10, this doesn't imply a more efficient utilization of the input energy for smelting, as a greater fraction of this energy is simply consumed for heating, leading to higher furnace temperatures.

Figure 12 shows a break-down of the total heat loss into the sidewall, bottom, roof, off-gas and cooling water (in percentage of the total heat loss) in a six-in-line furnace. It

can be seen from this figure that the furnace heat is mainly transported away by cooling water and off-gas. Of the total heat loss, for the total power input range (15–40 MW) investigated in this work, 35 to 45% is lost to the cooling water, about 33% to the off-gas, 10 to 15% through the furnace bottom and roof, and less than 5% through the refractory sidewalls (in contact with the matte bath and the solid charge layer). While the fractions of the total heat loss through the furnace bottom and refractory walls and to the off-gas all decrease with the increase of the power input, the fraction of the total heat loss to the cooling water increases with the increase of the power input. This demonstrates that at higher and higher power input levels, higher proportions of energy is consumed for simply heating the slag.

Influence of electric power input on slag temperature and freeze lining thickness

Figure 13 shows the predicted slag bath temperature, as a function of the total power input, in a particular electrode cell (no. 4 cell) in a six-in-line furnace. This figure indicates that there is a nearly linear relationship between power input and slag bath temperature. An increase in the power input by 10 MW will lift the slag temperature by 50 to 60°C.
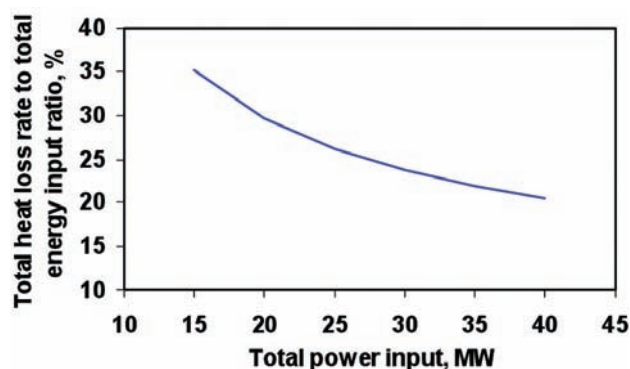

Figure 11—Predicted total heat loss rate as a percentage of total power input in a six-in line furnace
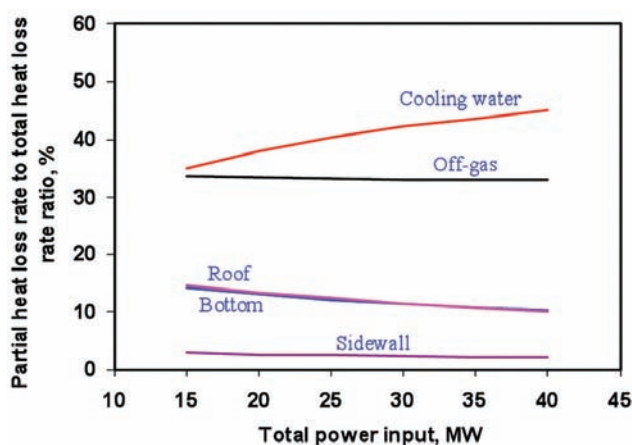

Figure 12—Predicted heat losses through different parts of a six-in-line furnace as percentages of the total heat loss

Mathematical modelling of heat transfer in six-in-line electric furnaces for sulphide smelting
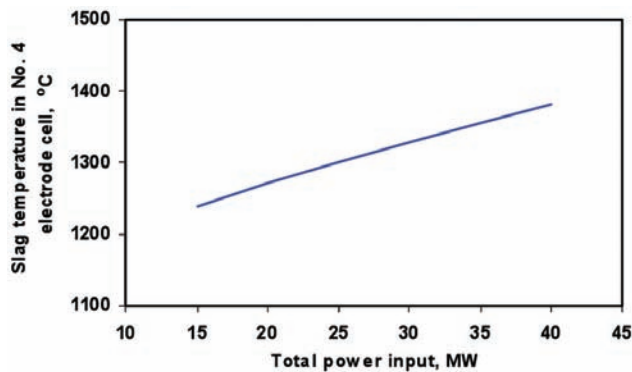

Figure 13—Influence of total power input on slag temperature in the no. 4 electrode cell in a six-in-line furnace

Figure 14 shows the model predicted freeze lining thickness, also as a function of the total power input, in the same electrode cell. It can be seen from this figure that the power input has a significant impact on the stability of the freeze lining. A higher power input leads to a thinner freeze lining. For instance, an increase of the power input by 10 MW can decrease the freeze lining thickness by 17 to 45 mm (or 20 to 30 per cent).

Influence of air gap formation on freeze lining thickness

In the present work, two limiting contact conditions between different solid material components in electric furnaces are assumed: (i) perfect contact and (ii) complete air gap formation between the freeze lining and the copper shell of the cooling unit. In the model, air gaps appearing in sidewalls of any electrode cells can be taken into account. Figure 15 shows the predicted freeze lining thickness in the sidewalls of a six-in-line furnace. It is assumed that a complete air gap is formed between the freeze lining and the cooling unit in the sidewall of the no. 4 electrode cell, while perfect contacts are assumed for the sidewalls of all the rest of the electrode cells. We can see from this figure that, compared with other electrode cells, an air gap formation can cause a decrease in freeze lining thickness (due to remelting) by more than half of its original thickness. Thus, an air gap has a marked impact on the stability of the freeze lining and its formation could be one of the significant root causes for the failure of cooling units in electric furnaces.

Influence of cooling parameters on freeze lining thickness

Figure 16 shows the influences of cooling water flow rate and inflow water temperature on the freeze lining thickness in the no. 4 electrode cell. It can be seen from this figure that, below about 4 kg/s, the cooling water flow rate has a significant influence on the freeze lining thickness; above this value, however, the effect of cooling water flowrate diminishes. The inflow water temperature has a limited effect on the freeze lining thickness. A decrease of this temperature from 60°C to 20°C results in an increase of freeze lining thickness by only 4 to 5 mm.

Compared with Figures 14 and 15, it can be seen from these results that the power input and complete air gap formation have much larger impacts on the freeze lining thickness than the cooling parameters (such as water flow rate and inflow water temperature). Nevertheless, this doesn't
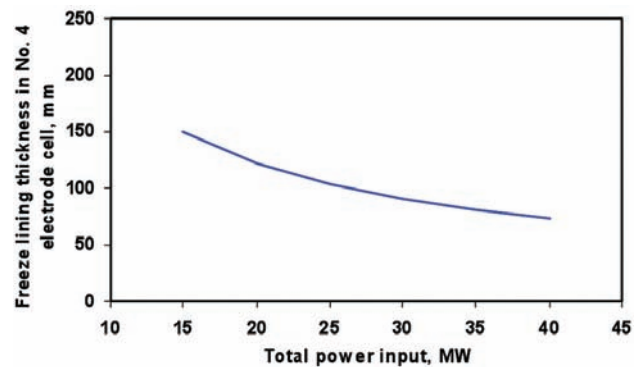

Figure 14—Influence of total power input on freeze lining thickness in No. 4 electrode cell in a six-in-line furnace
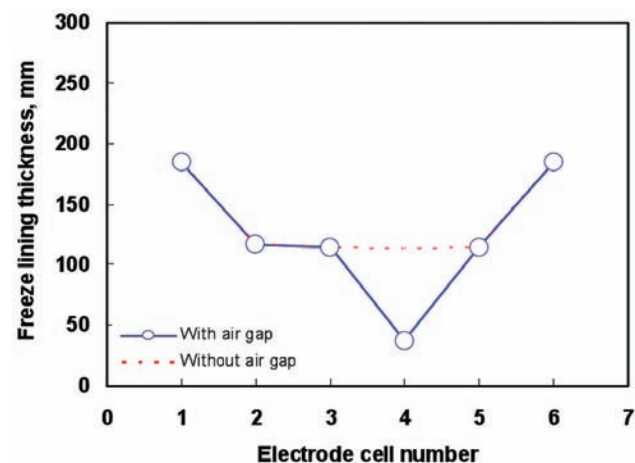

Figure 15—Influence of air gap formation on freeze lining thickness in the no. 4 electrode cell in a six-in-line furnace
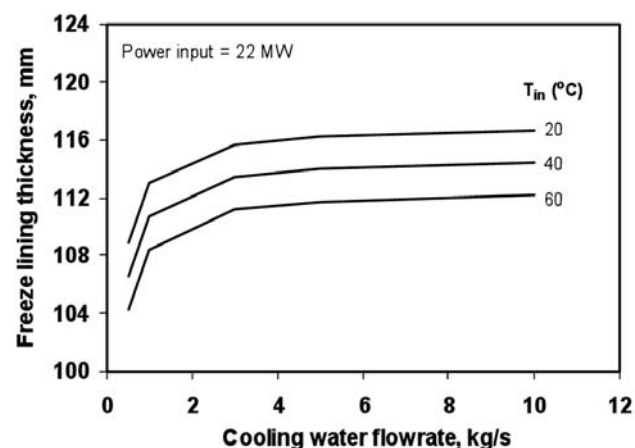

Figure 16—Influence of cooling water flow rate and inflow water temperature on freeze lining thickness in the no. 4 electrode cell in a six-in-line furnace

Mathematical modelling of heat transfer in six-in-line electric furnaces for sulphide smelting

mean these cooling parameters are unimportant. In fact, it is crucial to maintain the water temperature low enough inside the cooling units, by applying a high enough water flow rate and as low as possible inflow water temperature, so as to avoid water boiling inside the cooling units which can lead to explosion accidents. For a given inflow water temperature, this situation can be effectively avoided by keeping water flow rate above certain threshold values, depending on furnace power input. Figure 17 gives the predicted threshold water flow rates below which the water with different initial temperatures (at 20°C, 40°C, and 60°C respectively) could boil inside the cooling unit. In addition, the inflow water temperature affects the slope of the critical line shown in Figure 17. A lower inflow water temperature decreases this slope and thus reduces the 'boiling zone' in the figure.

It should be mentioned here that the assumptions of steady-state heat transfer and, in particular, perfect contact between the freeze lining and the cooling unit, are not expected to always hold in industrial furnaces. Thus, the above results may not be reliably used directly for real processes. This is because, as mentioned earlier, air gap formation will also have a marked influence on heat transfer to the cooling unit and hence the threshold water flow rate.

Influences of slag bath and solid charge heights on specific power consumption in a six-in-line furnace

Figures 18 and 19 show, respectively, the influences of changing the heights of slag bath and solid charge layer on the specific power consumption, under the same total power input condition. We can see from these figures that an increase in slag bath height results in an increase of heat loss to cooling water and thus leads to increased specific power consumption. According to Figure 18, a decrease in slag bath height by 100 mm could save energy by about 5 kWh for smelting one ton of solid charge. Figure 19 indicates that a thicker solid charge would work as a thermal insulation layer in electric furnaces. This is rather advantageous for reducing the heat loss and therefore decreasing the specific power consumption. According to this figure, an increase of the solid charge layer thickness by 100 mm could decrease the energy consumption by 8 to 18 kWh for smelting one ton of solid charge, but this effect on energy saving tends to decrease for thicker solid charge layers. In general, the results shown in Figures 18 and 19 suggest that maintaining a shallower slag bath and a thicker solid charge layer above it would be favourable for minimizing the specific power consumption in electric furnace operations.

Optimization of electric power input in a six-in-line furnace

As shown in Figure 7, in six-in-line furnaces a uniform power input to the electrodes can lead to noticeably cold regions in the end electrode cells. This could be regarded as a major cause for the precipitation of chromite spinel particles in the slag bath in some South African electric furnaces smelting UG2 ores, as depicted in Figure 1. With the help of

the present heat transfer model, it could be possible to minimize such spinel precipitation through optimizing the power input to the electrode cells in six-in-line furnaces, so
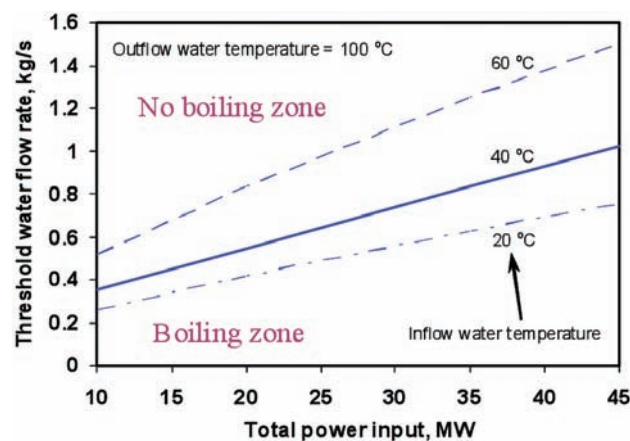

Figure 17—Threshold cooling water flow rate, as a function of power input, required to avoid water boiling inside the cooling unit
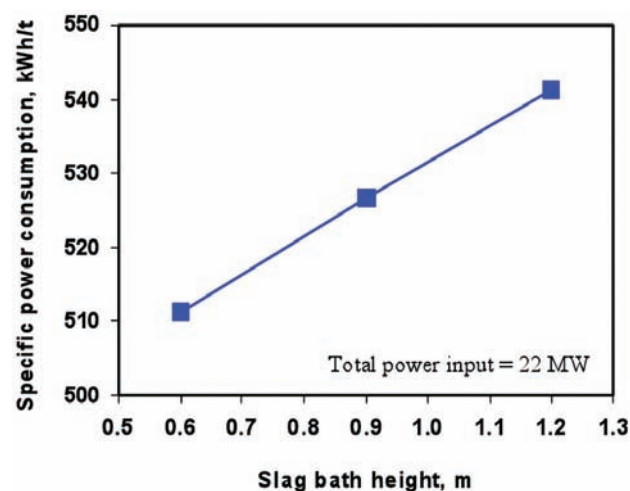

Figure 18—Influences of variation in slag bath height on specific power consumption in a six-in-line furnace
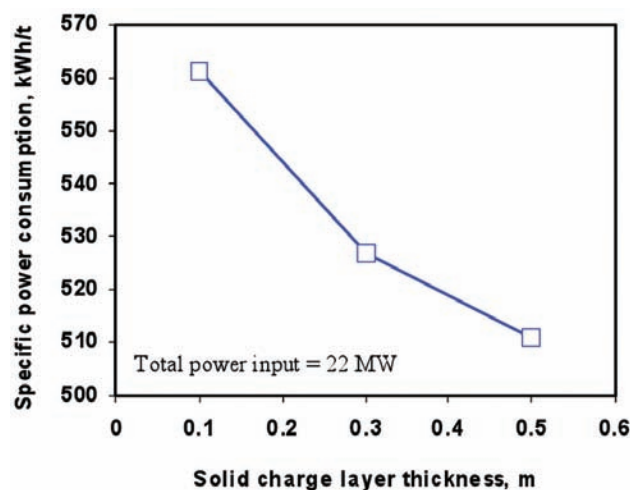

Figure 19—Influences of variation in solid charge layer thickness on specific power consumption in a six-in-line furnace

Mathematical modelling of heat transfer in six-in-line electric furnaces for sulphide smelting

as to realize more uniform heating in the furnaces. Figure 20 illustrates an example of using the model to find out an appropriate partition of the total electric power input to the six electrode cells to maintain a nearly even temperature distribution along the length of the furnace. In this work, modelling analysis was carried out on the effect of various controlling factors. As seen from Figure 20, adjusting the power input to the two end electrode cells (no. 1 and no. 6 cells) is quite effective. Nevertheless, the results shown in Figure 20 are just to elucidate one capability of the model in controlling power inputs to different electrode cells. The model doesn't suggest how to realize the optimum power input in practice and what side effects it would cause. One foreseeable effect would be that, if deeper electrode immersion depths were applied in the end electrode cells, more intensive bath agitation, due to more electrode gas stirring, could be expected in these cells.

This would be beneficial, since it would stir up the precipitated spinel deposits but, on the negative side, it would increase the electrode consumption rate, decrease the freeze lining thickness, and result in too hot a freeboard releasing

(a) Optimized power input in comparison with uniform power input in six-in-line furnace

(b) Temperature distributions along the length of six-in-line furnace for uniform and optimized power inputs shown in the above figure

Figure 20—Comparisons of slag temperature distribution along the length of a six-in-line furnace for optimized power input with that for uniform power input

increased amounts of hot electrode gases, etc. In all, this is an area for further more detailed studies.
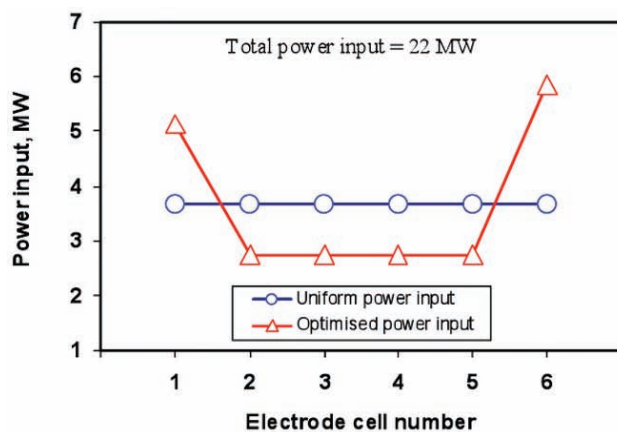
Conclusions

Based on the concept of heat transfer in multilayer composite material systems, an efficient and portable mathematical model for simulating heat transfer in six-in-line electric furnaces has been developed. The model has the following capabilities:
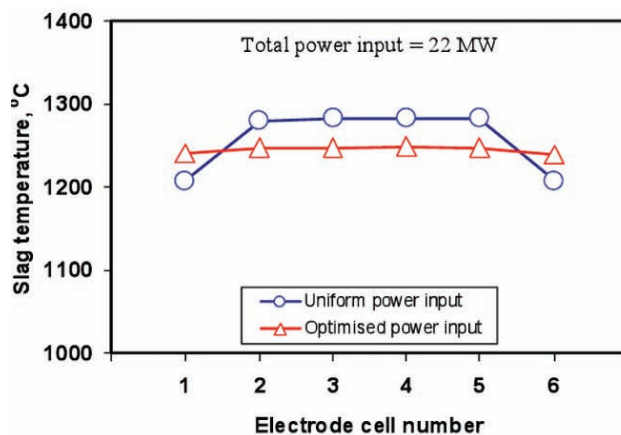
(1) Prediction of average temperatures in any material component (such as slag, matte, solid charge, freeze lining, and refractory lining etc.) and at any interface formed by two material components in the furnace
(2) Prediction of freezing lining thickness with or without air gap formation
(3) Prediction of smelting rate and heat loss rates
(4) Prediction of the lowest specific power consumption
(5) Optimization of power distribution in electrode cells
(6) Online implementation on industrial electric furnaces.

From the modelling results, the following conclusions can be drawn:

➤ In six-in-line furnaces, a uniform power input to the electrodes leads to noticeably higher slag temperatures in the middle electrode cells compared with the end electrode cells and, accordingly, a much thinner freeze lining in the middle cells than in the end cells. Therefore, more care should be taken in the cooling of the middle cells in six-in-line furnaces.

➤ The freeze lining thickness is significantly influenced by the power input and air gap formation between the freeze lining and cooling unit (assuming perfect contact between all the other material components). Formation of a complete air gap can lead to a reduction of the freeze lining by more than half of its original thickness

➤ For the water cooling units in electric furnaces, to avoid water boiling inside the units there exists a threshold water flow rate that is nearly linearly proportional to the total power input, with a slope depending on the inflow water temperature. A lower inflow water temperature decreases this slope, allowing a lower water flow rate for furnace cooling to be used

➤ The furnace charge smelting rate is nearly linearly proportional to the total power input. However, in terms of power consumption for smelting per unit amount of solid charge (specific power consumption), there exists a minimum specific power consumption and hence a limited smelting rate or productivity within a certain range of power input. Therefore, a compromise between specific power consumption and productivity to manage a profit is recommended in practice

➤ Of the total furnace heat loss, 35 to 45 per cent is carried away by the cooling water and about 33 per cent by the off-gas, which comprise a significant amount of thermal energy that could be recovered and reused

Mathematical modelling of heat transfer in six-in-line electric furnaces for sulphide smelting

➤ A shallower slag bath and a thicker layer of solid charge would be favourable for reducing heat losses to cooling units and to freeboard, and hence decreasing the specific power consumption

➤ In order to achieve uniform heating in six-in-line furnaces by minimizing the low temperature regions in the end electrode cells, a non-uniform and optimized power input to the electrode cells would be beneficial. That is, for the same total power input, the end electrode cells should receive higher heating power than the middle electrode cells. However, in practice, one should be cautious about possible side effects due to the significant increase of power input into the end electrode cells, such as increased electrode consumption and intensified bath agitation in these electrode cells.

Acknowledgement

Appendix: nomenclature

Alphabetic symbols

A	Heat transfer area (m²)
A_{sw}	Heat transfer area between freeze lining and cooling unit (m²)
C_{pc}	Heat capacity of solid charge (J/kg·K)
C_{pm}	Heat capacity of liquid matte (J/kg·K)
C_{ps}	Heat capacity of liquid slag (J/kg·K)
C_w	Heat capacity of water (J/kg·K)
D_w	Inner diameter of water pipe in cooling unit (m)
f	Heat transfer coefficient correction factor (dimensionless)
F_{ij}	View factor between radiative surfaces i and j (dimensionless)
Gr	Grashof number (dimensionless)
G_m	Matte production rate in an electrode cell (kg/s)
G_s	Slag production rate in an electrode cell (kg/s)
G_{smelt}	Solid charge melting rate in an electrode cell (kg/s)
G_w	Cooling water flow rate (kg/s)
h	Convection heat transfer coefficient (W/m²·K)
H_{smelt}	Heat consumed for smelting per unit mass of solid charge (J/kg)
k	Thermal conductivity (W/m·K)
k_{ss}	Thermal conductivity of freeze lining (W/m·K)
L	Thickness of a material layer (m)
L_{freeze}	Freeze lining thickness (m)
L_{pipe}	Total length of water pipe in cooling unit (m)
Nu	Nusselt number (dimensionless)
Pr	Prandtl number (dimensionless)
Q_c	Heat flow rate for heating the solid charge (W)
Q_{c-cond}	Net conduction heat flow rate in solid charge from the neighbouring electrode cells (W)
Q_{cf}	Convection and radiation heat flow rate from the top surface of the solid charge to the freeboard space (W)
$Q_{droplets}$	Net sensible heat flow rate contributed by the descending slag and matte droplets produced at the slag/charge interface (W)
Q_{gas}	Net heat flow rate absorbed by solid charge from the reaction gases generated by smelting at the slag/charge interface (W)
Q'_{gas}	Net heat flow rate transported by the reaction gases evolving through the solid charge layer to the freeboard space (W)
Q_{g-conv}	Net convection heat flow rate transported by bulk off-gas flow in the freeboard space from the neighbouring electrode cells (W)
$Q_{ingress-air}$	Rate of heat absorbed by ingress air in the freeboard space (W)
Q_{input}	Effective electric energy input rate (power) into slag bath in an electrode cell (W)
Q_m	Heat flow rate for heating the newly produced matte droplets (W)
Q_{m-conv}	Net convection heat flow rate transported by bulk matte flow from the neighbouring electrode cells (W)
$Q_{m-droplets}$	Sensible heat flow rate contributed by matte droplets descending from the slag bath (W)
Q_s	Heat flow rate for heating the newly produced slag droplets (W)
Q_{sc}	Convection heat flow rate from slag bath to slag/charge interface (W)
Q_{scc}	Conduction heat flow rate from slag/charge interface to the centre of the solid charge layer (W)
Q_{s-conv}	Net convection heat flow rate transported by bulk slag flow from the neighbouring electrode cells (W)
Q_{sm}	Convection heat flow rate from slag bath to matte bath (W)
Q_{smelt}	Net heat flow rate consumed for smelting the solid charge (W)
Q_{sw}	Convection heat flow rate from slag bath to the surface of freeze lining layer (W)

Mathematical modelling of heat transfer in six-in-line electric furnaces for sulphide smelting

R	Heat transfer resistance (K/W)
R_{cw}	Heat transfer resistance between copper and water in cooling unit (K/W)
Re	Reynolds number (dimensionless)
R_{sc}	Convection heat transfer resistance at the slag/charge interface (K/W)
R_{scc}	Conduction heat transfer resistance between the slag/charge interface and the centre of the solid charge layer (K/W)
T	Temperature (K)
T_a	Ambient (atmosphere or room) temperature (K)
T_b	Boundary temperature (K)
T_{bulk}	Temperature of bulk material (K)
T_c	Temperature at centre of the solid charge layer (K)
T_{cw}	Temperature at copper/water interface in cooling unit (K)
T_f	Temperature of bulk off-gas in the freeboard space (K)
T_m	Temperature of bulk matte (K)
T_s	Temperature of bulk slag (K)
T_{smelt}	Temperature at the slag/charge interface, i.e. smelting zone (K)
T_{sol}	Solidus of freeze lining, i.e. solid slag, (K)
T_{surf}	Temperature at material surface (K)
$T_{surf,i}$	Temperature at material surface i (K)
$T_{surf,j}$	Temperature at material surface j (K)
T_{sw}	Temperature of the cold face of the freeze lining layer (K)
$T_{w,in}$	Temperature of water flowing into cooling unit, (K)
$T_{w,out}$	Temperature of water flowing out of cooling unit, (K)

Greek symbols

ε	Surface emissivity (dimensionless)
σ	Stefan-Boltzmann constant (= 5.6703×10^{-8} W/m$^2 \cdot$K^4)
μ_0	Viscosity of fluid at interface (Pa·s)
μ_b	Viscosity of bulk fluid (Pa·s)

Common subscripts

i	Index number of material component
j	Index number of heat transfer direction
w	Subscript for water cooling parameters

References

1. CRAMER, L.A. The extractive metallurgy of South Africa's platinum ores. *Journal of Metals*, 2001. pp. 14–18.

2. NELL, J. Melting of platinum group metals concentrates in South Africa. Proceedings of the VII International Conference on Molten Slags, Fluxes and Salts, Cape Town, South Africa, 25–28 January 2004. Johannesburg, *The Southern African Institute of Mining and Metallurgy*. pp. 165–170.

3. URQUHART, R.C., RENNIE, M.S., AND RABEY, C.C. The smelting of copper-nickel concentrates in an electric furnace. Proceedings of Extractive Metallurgy of Copper: vol. 1. Pyrometallurgy and Electrolytic Refining. Yannopoulos, J.C. and Agarwal, J.C. (eds.). Warrendale, Pennsylvania, *The Metallurgical Society of AIME*, 1976. pp. 275–295.

4. SHENG, Y.Y. and IRONS, G.A. Mathematical and physical modelling of fluid flow and heat transfer in electric smelting. *Canadian Metallurgical Quarterly*, vol. 37. no. 3–4, 1998. pp. 265–273.

5. SHENG, Y.Y., IRONS, G.A., and TISDALE, D.G. Transport phenomena in electric smelting of nickel matte: Part 1. Electric potential distribution. *Metallurgical and Materials Transactions B*, vol. 29B, 1998. pp. 77–83.

6. SHENG, Y.Y., IRONS, G.A., and TISDALEI, D.G. Transport phenomena in electric smelting of nickel matte: Part 2 .Mathematical modelling. *Metallurgical and Materials Transactions B*, vol. 29B, 1998. pp. 85–94.

7. JARDY, A., ABLITZER, D., and JORGET, S. Modelling of slag behaviour in a non-ferrous smelting electric furnace. *Proceedings of the Reinhardt Schumann International Symposium on Innovative Technology and Reactor Design in Extraction Metallurgy*. TMS-AIME Fall Meeting for Extractive and Process Metallurgy, Colorado Springs, Colorado, 9–12 November 1986. Gaskell, D.R., Hager, J.P., Hoffmann, J.E., and Mackey, P.J. (eds.). pp. 419–431.

8. XIA, J.L. and AHOKAINEN, T. Numerical modelling of slag flows in an electric furnace. *Scandinavian Journal of Metallurgy*, vol. 33, no.4, 2004. pp. 220–228.

9. PAN, Y., SUN, S., and JAHANSHAHI, S. Efficient and portable mathematical models for simulating heat transfer in electric furnaces for sulphide smelting. Proceedings of the Sohn International Symposium on Sulphide Smelting, San Diego, California, 27–31 August 2006. Kongoli, F. and Reddy, R.G. (eds.). Warrendale, Pennsylvania, *The Minerals, Metals and Materials Society*. pp. 599–613.

10. GEIGER, G.H. and POIRIER, D.R. Transport Phenomena in Metallurgy. Addison-Wesley, Reading, Massachusetts, 1973.

11. ROHSENOW, W.M. and CHOI, H.Y. Heat, Mass and Momentum Transfer. Prentice-Hall, Englewood Cliffs, New Jersey, 1961.

12. WEAST, R.C., ASTLE, M.J., and BEYER, W.H. (eds.). CRC Handbook of Chemistry and Physics. 64th edn. *CRC Press*, Boca Raton, Florida, 1983–1984.

13. WHITAKER, S. Forced convection heat transfer correlations for flow in pipes, past flat plates, single cylinders, single spheres, and for flow in packed beds and tube bundles. *AIChE Journal*, vol. 18, no. 2, 1972. pp. 361–371 ◆